中國機械工程學刊第三十九卷第三期第 287~293 頁(民國一百零七年)
Journal of the Chinese Society of Mechanical Engineers, Vol.39, No.3, pp 287~293 (2018)

Crack Formation and Corrosion Behavior of 6061 Al Alloy in Sulfuric Acid

I-Chun Chung*, Chen-Kuei Chung**and Yan-Kuin Su***

Keywords：Anodic aluminum oxide; Crack; Corrosion; AA6061.

ABSTRACT

The 6061 aluminum alloys (AA6061) specimens were anodized in the sulfuric acid solution. The crack formation and corrosion behavior of the AA6061 oxide films were investigated in a wide range of sulfuric acid concentration (1~5 M) and current density (0.3~3 A/dm^2). A number of cracks were formed on the surface of the anodized AA6061 oxide film at a high electrolyte concentration of 5 M and low current density of 0.3 A/dm^2. Moreover, increasing current density could suppress crack formation at a high concentration of 5 M while decreasing electrolyte concentration was also helpful for eliminating cracks at a constant current density of 1 A/dm^2. The more the cracks, the higher the corrosion current was. Suppressing crack formation was crucial for promoting corrosion resistance of the AA6061 film with less corrosion current. The best corrosion resistance of the anodized film with $I_{corr}=1.433\times10^{-10}$ A/cm^2 was obtained at a current density of 1 A/dm^2 and a concentration of 1 M sulfuric acid, that could be potentially used for long-term anti-corrosion coatings on many AA6061 alloy products.

INTRODUCTION

The aluminum-based alloy is the second production less than the categories like iron-based alloy in the world. It is applied to a number of construction, automobile and aerospace industry due to light weight, high strength, high ductility, non-magnetic and good machinability for sophisticated parts. In addition, the aluminum alloy can be recycled in the used metal alloys, and it is in agreement with environmental requirements (Din et al., 2015; Zheng et al., 2015). The 6061 aluminum alloys (AA6061, Al-Mg-Si alloy) is one of the most popular commerce available aluminum alloys. It is one of the most reactive metallic elements, especially the addition of magnesium elements. Although the aluminum alloy formed oxide film with oxygen in the air will enhance corrosion resistance but it is not enough to meet the needs in the industry. More methods of surface treatment and coating were used to improve the corrosion resistance of aluminum alloy including laser surface melting (Viejo et al., 2010; Embuka et al., 2017), sputter deposited (D-Crespo et al., 2009; Liu et al., 2015), thermal sprayed coating (Pardo et al., 2009), electroless plating (Yin and Chen, 2013; Fetohi et al., 2015), micro-arc oxidation (Shen et al., 2013; Tran et al., 2017), and anodic aluminum oxide (Dejun and Jinchun, 2015; Wen et al., 2014). The laser source is very expensive at laser surface melting equipment. The sputter deposit is performed in a vacuum environment. The equipment of anodic processing is simple, low cost, and high stability so that it is popular in the industry. The different electrolytes in the anodic coating can be distinguished to oxalic acid, phosphoric acid, and sulfuric acid (Zaraska et al., 2010). The most common acid used for aluminum alloy anodizing is sulfuric acid, because the sulfuric acid is not only obtained easily but also can form the barrier layer quickly. It is noted that the cracks in the anodized film will affect the corrosion resistance results and of interest to study how the cracks are formed and suppressed (Haruna et al., 2005; Rosliza et al., 2008). In this article, we have investigated the AA6061 anodization at 1~5 M sulfuric acid concentration and 0.3~3 A/dm^2 current density for the evolution of crack formation and suppression. A potentiostatic polarization method was adopted to evaluate corrosion characteristics of metal specimens. In a typical polarization curve, lower corrosion current density corresponded to lower corrosion rate and better corrosion resistance of the coating. The best corrosion resistance of the anodized film with $I_{corr}=1.433\times10^{-10}$ A/cm^2 could be obtained at 1 A/dm^2 current density and 1 M sulfuric acid.

Paper Received April, 2017. Revised May, 2017. Accepted June, 2017. Author for Correspondence: Chen-Kuei Chung.

* *Gradnate Student, Department of Mechanical Engineering, National Cheng Kung University, Tainan 70101, Taiwan, ROC /Metal Industries Research & Development Centre, Kaohsiung, Taiwan 81160, ROC.*

** *Professor, Department of Mechanical Engineering and Center for Micro/Nano Science and Technology, National Cheng Kung University, Tainan, Taiwan 70101, ROC.*

*** *Emeritus Professor, Department of Electrical Engineering, National Cheng Kung University, Tainan, Taiwan 70101, ROC.*

EXPERIMENTAL PROCEDURE

The chemical composition of the used AA6061 alloy was listed in Table 1. The rectangular samples (Alcoa, 100 × 40 × 1 mm^3) were used as substrates in the experiment. In order to obtain a clean and smooth surface for uniformly electrical field during AA6061 anodized procedures. The samples were polished with sandpapers #800, #1200, and #2000 and then ultrasonically degreased in the acetone and isopropyl alcohol for 15 min. The samples were alkali-washed in a 1 M sodium hydroxide solution for 10 min and then were ultrasonically washed in deionized water for 15 min to remove the oxide layers of specimens. Finally, these samples were dipped in 1 M H_2SO_4 to remove aluminum hydroxide residue and rinsed with deionized water to remove the residual H_2SO_4 to get the clean surface.

The anodization apparatus for anodic aluminum oxide (AAO) process is shown in Figure 1(a). It consisted of double-layer electrode system. In this system, the AA6061 sheet was immersed in the center of electrolyte as the working electrode. Two Ti alloy plates mounted on the inner surface of the tank were used as a counter electrode. The distance was 4 cm from the working electrode to counter electrode. The anodization process was controlled at 25 °C for 30 min in a cooling water system electrochemical cell containing diluted sulfuric acid with magnetic stirrer. The anodization process in this experiment was under a constant constant-current mode so the voltage varied with anodizing time. We used five AA6061 alloy samples, namely A, B, C, D and E, for anodizing in the sulfuric acid solution under different anodization coating conditions over a wide range of current densities (1~3 A/dm^2) and sulfuric acid concentration (1~5 M) to study the surface morphology under crack suppression as well as corrosive behavior. The anodization conditions are listed in Table 2.

The microstructure and thickness of anodized AA6061 films were examined by using scanning electron microscopy (SEM, Hitachi S-3000N, Japan). The surface composition of the anodized samples was analyzed by using Energy Dispersive X-ray Spectrometer (EDX). The EDX which was attached to SEM. The corrosion resistance of the anodized films was evaluated by potentiostatic apparatus shown in Figure 1(b). The corrosion behavior of all samples was carried out in a 3.5 wt.% NaCl solution at room temperature. The system composed of a potentiostat and a three-electrode cell system. The three-electrode system comprised an AAO sample as the working electrode (WE) which exposed to solution was 1.3cm^2, a platinum sheet as the counter electrode (CE), and a saturated calomel electrode as the reference electrode (RE). During the electrochemical test, the polarization curve of the AAO sample was gained by recording the voltage or current value. Electrochemical parameters including corrosion potentials (E_{corr}) and corrosion current densities (I_{corr}) were determined from the intersection of the linear anodic and cathodic of the polarization curves. The value of corrosion potential was determined as the voltage when corrosion stared as the corrosion potential was higher the coated AAO films had lower activity, and had less susceptible to corrosion. The value of corrosion current densities represented the corrosion rate. The smaller anodic current density usually implied lower corrosion rate, and had the higher corrosion resistance.

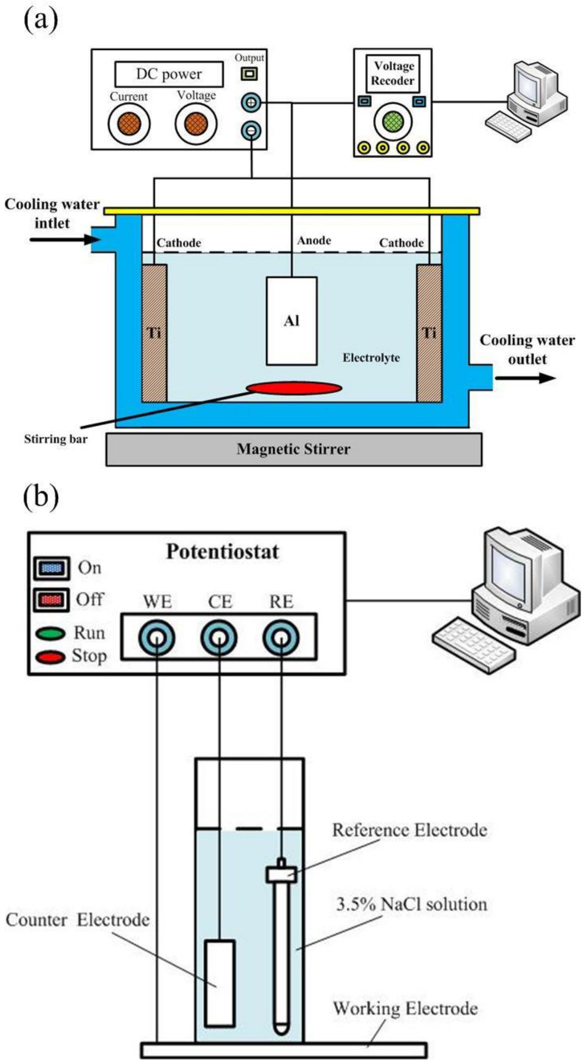

Fig. 1. Schematic diagram of the (a) the double-layer electrolyte system of anodization apparatus and (b) the three-electrode cell system of potentiostat apparatus.

Table 1 Chemical composition of AA6061 alloy (wt %).

Mg	Si	Fe	Cu	Cr	Ti	Mn	Zn	Al
1.00	0.64	0.50	0.24	0.16	0.06	0.04	0.01	Bal.

Table 2 Thin film forming conditions and the resulting thin-film thickness as well as the corrosion potential and corrosion current density values of the anodized coatings.

	Thin-film formation conditions			Sample test results		
Specimen No.	Current density (A/dm^2)	Sulfuric acid concentration (M)	Reaction time (min)	Thickness (μm)	E_{corr} (V vs.SCE)	I_{corr} (A/cm^2)
A	0.3	5	30	1.78	-1.5014	1.058×10^{-8}
B	1	5	30	8.54	-1.1665	3.759×10^{-9}
C	3	5	30	26.53	-1.0248	7.936×10^{-10}
D	1	3	30	7.97	-1.1736	1.234×10^{-9}
E	1	1	30	7.86	-1.2031	1.433×10^{-10}
F	3	1	30	24.30	-1.0766	2.621×10^{-10}

RESULTS AND DISCUSSION

The voltage – time behaviors of the anodization of the AA6061 samples over a wide range of current densities (0.3~3 A/dm^2) and concentration (1~5 M) in sulfuric acid are shown in Figure 2. In the anodization process, the current density was constant and the voltage was recorded. The voltage-time curves for anodizing AA6061 in sulfuric acid electrolyte was performed for 30 min to understand the crack formation and the anodizing oxidation behavior. In general, the voltage of the anodization process can be divided into three stages. The 1st stage is the barrier-layer formation, during which the voltage rose suddenly to a maximum voltage. In the 2nd stage, the voltage from the maximum value decreased gradually with time due to the formation of the porous layer. The abrupt decrease in duration was related to the porous-layer density stacking, while the shorter duration corresponds to the less-dense porous layer. If the porous-layer formation was not obvious from the maximum voltage to steady voltage, cracks were formed. In the 3rd stage, the voltage was in the steady stage, and the thickness of porous layer increased stably as the voltage remained constant. Samples A, B and C anodized at the different current densities of 0.3, 1 and 3 A/dm^2 at the constant concentration of 5 M were compared. Sample A has no obvious porous-layer from the maximum voltage to steady voltage, and it was noticed that cracks were formed. Sample C had a short 2nd stage reaction time compared to the other samples. This implies that the formation of the porous layer structure is less dense than the others in the 2nd stage. According to Ohm's law, the voltage is proportional to the current when the resistance is constant. The stable voltages of samples A, B and C were 3.6, 7.1 and 11.9 V, respectively. The stable voltage is proportional to the applied current density. AA6061 samples B, D and E were anodized in electrolytes with the different concentrations of 5, 3 and 1 M sulfuric acid at a constant current density of 1A/dm^2. The stable voltages of the samples B, D and E were 7.1, 8.9 and 15.4 V, respectively. Either the higher concentration caused higher conductivity or the lower resistance in the sulfuric acid electrolyte resulted in a lower stable voltage. At the same current density, the final anodic voltage decreased with increasing electrolyte concentration

Figure 3 shows the cross-sectional SEM images of samples A, B, C, D and E under the different conditions as listed in Table 2. Due to the significant difference in thickness, the SEM was conducted with different amplification bars. For example, the sample C is very thick, and so needs a larger ratio scale bar to view the entire film. In comparing samples A, B and C anodized at the different current densities of 0.3, 1 and 3 A/dm^2 with a constant concentration of 5 M, it can be seen that the oxidized film thicknesses increased with current density, and measured 1.78, 8.54 and 26.53 μm for samples A, B and C, respectively, as listed in Table 2. The thickness of the films was approximately proportionate to the applied current density. Comparing samples B, D and E anodized at the different concentration of 5, 3 and 1 M sulfuric acid at the fixed current density of 1 A/dm^2, it was found that the film thicknesses of samples B, D and E were 8.54, 7.97 and 7.86 μm, respectively, as listed in Table 2. From the result, it is clear that the thickness did not changed greatly due to different sulfuric acid concentrations.

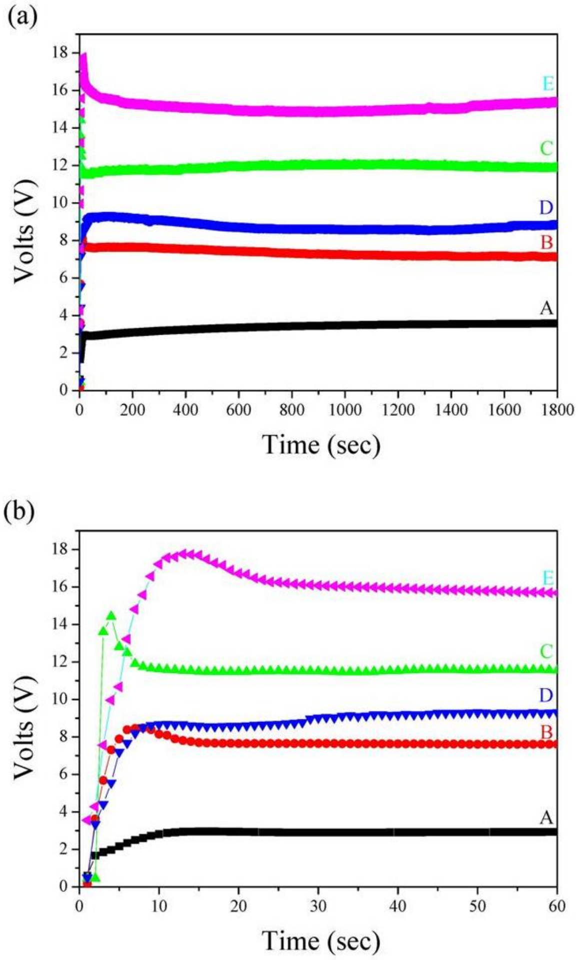

Fig. 2. Voltage–time curves for anodizing AA6061 under different anodized conditions. The current densities and sulfuric acid concentrations for samples: (A) 0.3 A/dm^2, 5M; (B) 1 A/dm^2, 5M; (C) 3 A/dm^2, 5M; (D) 1 A/dm^2, 3M; and (E) 1 A/dm^2, 1M; (a)Total reaction time of 0–1800sec, and (b) the initial reaction time from 0–60sec.

Figure 4 shows the planar–view SEM images of samples A, B, C, D and E films anodized under various conditions. Cracks had formed on the surface of the anodized AA6061 oxide film with high concentration and low current density. Numerous cracks with a network-like distribution were found in sample A; in contrast, sample B with an increased current density had clear cracks, but fewer than sample A. As the current density increased to 3 A/dm^2 (sample C), cracks could not be observed. The current density enhanced the thickness of the anodic oxide with volume expansion leading to more compressive residual stress, which may have suppressed crack formation on the surface during anodization. Sample D had a few cracks on the film surface. No apparent cracks were observed for samples C and E. Compared to sample B at the constant current density of 1 A/dm^2, decreasing the sulfuric acid concentration in samples D and E appeared to reduce the formation of cracks.

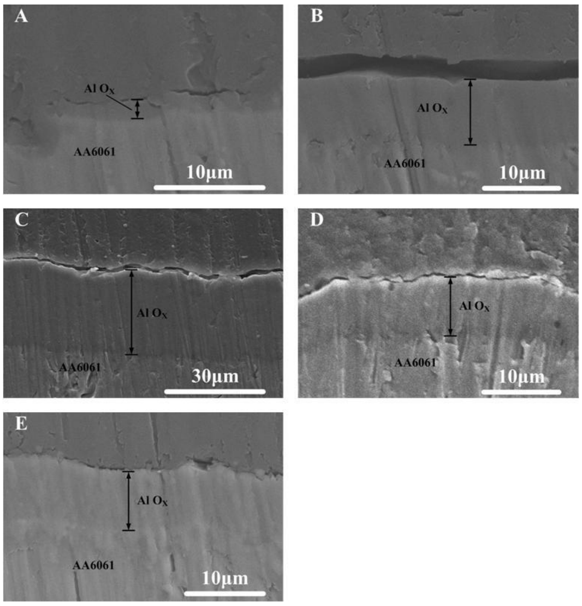

Fig. 3. Cross-sectional micrographs of the Al alloy films anodized under different conditions. The current densities and sulfuric acid concentrations for samples: (A) 0.3 A/dm^2, 5M; (B) 1 A/dm^2, 5M; (C) 3 A/dm^2, 5M; (D) 1 A/dm^2, 3M; and (E) 1 A/dm^2, 1M. The reaction time is 30 min

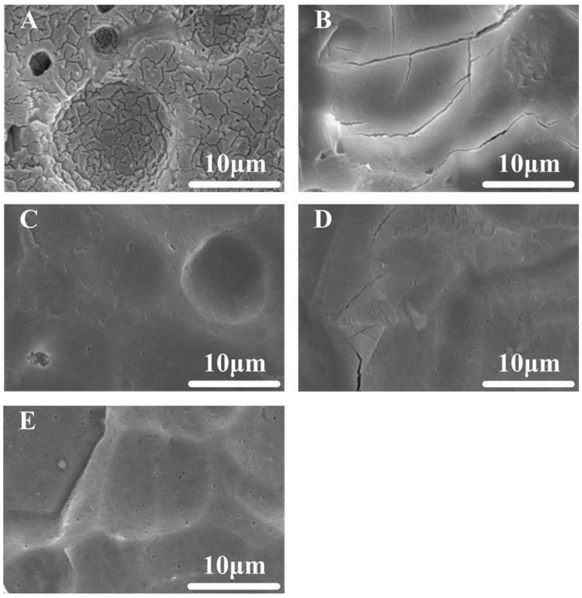

Fig. 4. SEM micrographs of Al alloy films anodized under different conditions. The current densities and sulfuric acid concentrations for samples: (A) 0.3 A/dm^2, 5M; (B) 1 A/dm^2, 5M; (C) 3 A/dm^2, 5M; (D) 1 A/dm^2, 3M; and (E) 1 A/dm^2, 1M. The reaction time is 30 min.

Table 3. Atomic composition of anodized coatings

Atomic （%）	A	B	C	D	E	F
O	52.94	67.25	68.03	64.70	62.61	62.19
Al	46.15	30.24	29.05	33.00	35.87	34.69
S	0.91	2.51	2.92	2.30	1.52	3.12
O/Al	1.15	2.22	2.34	1.96	1.75	1.79

In order to inspect the effects of composition of the anodized coating for the formation of cracks and corrosion resistance, the compositions of the anodized coating were analyzed by EDX, and are listed in Table 3. The EDX analyses indicated that the anodic oxide film contained O, Al and S elements. The atomic composition of the O element represents the formation of oxide in the form of aluminum oxide (AlO_x) and sulfuric oxide (SO_x) in the sulfuric acid solution. The atomic composition of the Al element represents the AA6061 alloy, while the atomic composition of the S element was from the sulfuric acid anodization system. The O/Al ratio of sample A was 1.15, which is less than the ratio of the Al_2O_3 phase. It was noticed that the AlO_x films were not sufficiently oxidized. The O/Al ratios for other samples were more than 1.5 of Al_2O_3 stoichiometry, because the higher O/Al ratios are contributed from SO_x. At the same current density of 1 A/dm^2, the S atomic ratios in samples B, D and E were 2.51, 2.30 and 1.52, respectively. Decreasing the sulfuric acid concentration also reduced the reaction rate of the AlO_x film, and lowered the S element content.

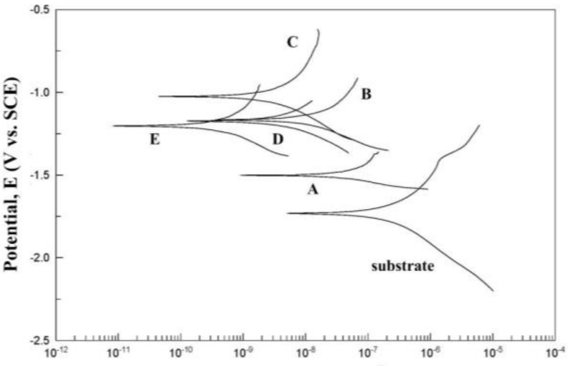

Fig. 5. Polarization curves of the anodized Al formed under different conditions. The substrate is AA6061. The current densities and sulfuric acid concentrations for samples: (A) 0.3 A/dm^2, 5M; (B) 1 A/dm^2, 5M; (C) 3 A/dm^2, 5M; (D) 1 A/dm^2, 3M; and (E) 1 A/dm^2, 1M.

The corrosion behaviors of the anodized AA6061 films formed under the different anodizing conditions were evaluated through the Tafel polarization method, the respective curves of which are shown in Figure 5. The results of polarization curves are the corrosion potential (E_{corr}) and the corrosion current density (I_{corr}), as listed in Table 2. With the higher sulfuric acid concentration of 5 M, increasing the current density from 0.3 to 3 A/dm^2 led to an enhanced growth rate and formed thicker oxide films and a more positive E_{corr} from –1.5014 to –1.0248 V vs. SCE, while reducing I_{corr} from 1.058×10^{-8} to 7.936×10^{-10} A/cm^2. At a same current density of 1 A/dm^2, decreasing the sulfuric acid concentration from 5 to 1 M led to a reduced reaction rate, and lowered the corrosion current density from 3.759×10^{-9} to 1.433×10^{-10} A/cm^2. Moreover, the corrosion resistance of samples C and E were much better than samples A, B and D. This indicates that the amount of the cracks is inversely proportional to the corrosion resistance.

We performed one more experiment on AAO sample F at the 1 M sulfuric acid concentration and 3 A/dm^2 current density to evaluate the crack formation and corrosion behavior. Figure 6(a) shows the voltage – time behavior for the initial reaction time from 0–60 sec on the anodized AA6061 film. Sample F had the maximum voltage and a shorter 1st stage reaction time compared to sample E. This implies that the formation of barrier-layer structure in the 1st stage at the higher current density of 3 A/dm^2 is less dense than that at 1 A/dm^2. Figure 6(b) presents the cross-sectional SEM images of sample F, the film thickness of which was 24.30 μm, as listed in Table 2. Figure 6(c) shows the planar-view SEM images of sample F; and as can be seen, it has no cracks on the film surface. The composition of sample F's anodized coating was analyzed by EDX, as listed in Table 3. Figure 6(d) shows the polarization curves of sample F as well as the E_{corr} and I_{corr} values, as listed in Table 2. With the lower sulfuric acid concentration of 1 M, the thickness of the anodized films in samples E and F were 7.86 and 24.30 μm, respectively, while the E_{corr} in samples E and F were –1.2031 and –1.0766 V vs. SCE. The thicker oxide layer led to more positive corrosion potential. The I_{corr} in samples E and F were 1.433×10^{-10} and 2.621×10^{-10} A/dm^2, repectively. This indicates that sample E had more anti–corrosion behavior than sample F with the lowest I_{corr}. Sample F was thicker than sample E; however, its corrosion resistance was inferior to that of sample E due to the less-dense barrier layer. As a result, the coating formed at the current density of 1 A/dm^2 and concentration of 1 M (sample E) showed the best corrosion resistance among the anodized coatings.

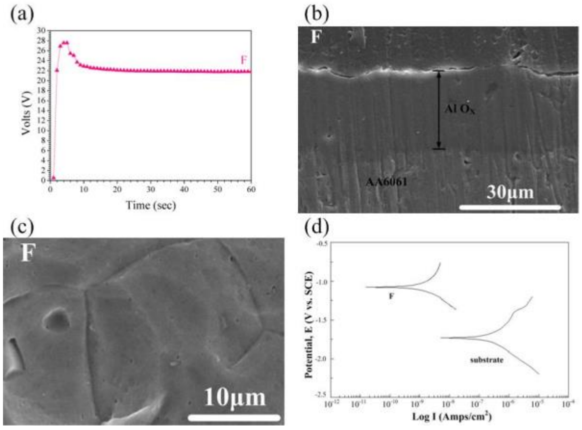

Fig. 6. AA6061 alloy films anodized at the current density of 3 A/dm^2, sulfuric acid concentration of 1 M, and reaction time of 30 min: (a) the voltage–time curves for the initial reaction time from 0–60 sec; (b) cross–sectional micrograph; (c) surface morphology; and, (d) the polarization curves.

CONCLUSIONS

We investigated the surface of AA6061 alloy anodized in the sulfuric acid for crack suppression and corrosive behavior. The effects of applied current densities and concentrations of sulfuric acid on the morphology of the cross-sectional and planar-views, oxide-film thickness, the composition of the oxide film and corrosion resistance of the anodized layer were characterized. The formation of surface cracks in the oxide film is related to the high sulfuric-acid concentration, which enhanced the reaction rate and thinned the layer thickness due to residual stress. Sample A has the most cracks, leading to poor corrosion resistance. The corrosion resistance needed to be enhanced to prevent crack formation. Two methods were then proposed to inhibit cracks forming in the anodic oxide film. One was to increase the current density to enhance the thickness in the oxide film with more compressive residual stress to inhibit crack formation. The other was to decrease the concentration of sulfuric acid to reduce the reaction rate and impede crack formation. The coating with the best corrosion resistance (I_{corr}=1.433×10^{-10} A/cm^2) was obtained by anodizing at a current density of 1 A/dm^2 and a concentration of 1 M sulfuric acid solution.

ACKNOWLEDGMENT

This work is partial sponsored by Ministry of Science and Technology (MOST) under contract No MOST105-2221-E-006-077.

REFERENCES

D-Crespo M. A., T-Huerta A. M., Rodil S. E., R-Meneses E., S-Velazquez G. G. and H-Perez M. A., “Effective corrosion protection of AA6061 aluminum alloy by sputtered Al–Ce coatings,” Electrochimica Acta 55 (2009) 498–503.

Dejun K., and Jinchun W., “ Salt spray corrosion and electrochemical corrosion properties of anodic oxide film on 7475 aluminum alloy,” Journal of Alloys and Compounds 632 (2015) 286–290.

Din R. U., Bordo K.B., Jellesen M.S., and Ambat R., “Accelerated growth of oxide film on aluminium alloys under steam: Part II: Effects of alloy chemistry and steamvapour pressure on corrosion and adhesion performance,” Surface and Coatings Technology. 276 (2015) 106–115.

Embuka D., Coy A.E., Hernandez-Barrios C.A., Viejo F., and Liu Z., “Thermal stability of excimer laser melted films formed on the AA2024-T351 aluminium alloy: Microstructure and corrosion performance,” Surface and Coatings Technology. 313 (2017) 214–221.

Fetohi A. E., Hameed R.M. A., El-Khatib K.M., “Development of electroless Ni–P modified aluminum substrates in a simulated fuel cell environment,” Journal of Industrial and Engineering Chemistry 30 (2015) 239–248.

Haruna T., Kouno T., and Fujimoto S., “Electrochemical conditions for environment-assisted cracking of 6061 Al alloy,” Corrosion Science 47 (2005) 2441–2449.

Liu Y., Huang J., Claypool J.B., Castano C. E., and O’Keefe M. J., “Structure and corrosion behavior of sputter deposited cerium oxidebased coatings with various thickness on Al 2024-T3 alloy substrates,” Applied Surface Science 355 (2015) 805–813.

Pardo A., Casajus P., Mohedano M., Coy A.E., Viejo F., Torres B., and Matykina E., “Corrosion protection of Mg/Al alloys by thermal sprayed aluminium coatings,” Applied Surface Science 255 (2009) 6968–6977.

Rosliza R., Senin H. B., and Nik W. B. W., “Electrochemical performances and corrosion inhibition of AA6061 in tropical seawater,” ASEAN Journal Science and Technology Development (AJSTD) 25 (2008) 251-259.

Shen D., Li G., Guo C., Zou J., Cai J., He D., Ma H., and Liu F., “Microstructure and corrosion behavior of micro-arc oxidation coatingon 6061 aluminum alloy pre-treated by high-temperature oxidation,” Applied Surface Science 287 (2013) 451–456.

Tran Q. P., Sun J. K., Kuo Y. C., Tseng C. Y., He J. L., and Chin T. S., “Anomalous layer-thickening during micro-arc oxidation of 6061 Al alloy,” Journal of Alloys and Compounds 697 (2017) 326–332.

Viejo F., Coy A.E., García-García F.J., Merino M.C., Liu Z., Skeldon P., and Thompson G.E., “Enhanced performance of the AA2050-T8 aluminium alloy following excimer laser surface melting and anodising processes,” Thin Solid Films 518 (2010) 2722–2731.

Wen Y., Meng H., and Shang W., “Influence of preparation temperature on the electrochemical characteristics of the Dodecafluoroheptyl-propyl-trimethoxysilane SAMs on aluminum alloy 6061,” Surface and Coatings Technology. 258 (2014) 574–579.

Yin Z., and Chen F., “Effect of nickel immersion pretreatment on the corrosion performance of electroless deposited Ni–P alloys on aluminum,” Surface and Coatings Technology. 228 (2013) 34–40.

Zaraska L., Sulka G. D., Szeremeta J., and Jaskuła M., “Porous anodic alumina formed by anodization of aluminum alloy (AA1050) and high purity aluminum,” Electrochimica Acta 55 (2010) 4377–4386.

Zheng S., Li C., Fu Q., Li M., Hu W., Wang Q., Du M., Liu X., and Chen Z., “Fabrication of self-cleaning superhydrophobic surface on aluminum alloys with excellent corrosion resistance,” Surface and Coatings Technology. 276 (2015) 341–348.

6061 鋁合金於硫酸溶液中進行陽極氧化處理的薄膜裂痕形成與耐腐蝕行為之研究

鍾逸駿
國立成功大學機械工程學系/財團法人金屬工業研究發展中心

鍾震桂
國立成功大學機械工程學系/微奈米科技研究中心

蘇炎坤
國立成功大學電機工程學系

摘 要

本文主要是使用 6061 鋁合金製作陽極氧化薄膜，採用硫酸當作陽極處理過程的電解液，探討在大範圍的硫酸濃度（1~5 M）與電流密度（0.3~3 A/dm^2）對於陽極氧化膜裂痕的形成以及耐腐蝕行為的影響。在高的硫酸濃度(5 M)與低的電流密度(0.3 A/dm^2)時，陽極氧化薄膜表面發現許多裂痕形成，當在較高的硫酸濃度時增加電流密度將抑制陽極氧化薄膜裂痕的形成；當電流密度固定在 1 A/dm^2 時降低硫酸濃度亦有助於消除裂痕。當裂痕數量越多時，腐蝕電流密度則越高代表耐蝕性越差，抑制裂痕的形成將導致腐蝕電流變小代表有助於耐蝕性能提升，本研究最佳耐蝕性是當電流密度為 1 A/dm^2，硫酸濃度為 1 M 時腐蝕電流密度為 $I_{corr}=1.433\times10^{-10}$ A/cm^2。